

Tuning grain boundary cation segregation with oxygen deficiency and atomic structure in a perovskite compositionally complex oxide thin film

Cite as: Appl. Phys. Lett. **124**, 171605 (2024); doi: [10.1063/5.0202249](https://doi.org/10.1063/5.0202249)

Submitted: 2 February 2024 · Accepted: 13 April 2024 ·

Published Online: 25 April 2024



View Online



Export Citation



CrossMark

Huiming Guo,¹ Hasti Vahidi,¹ Hyojoo Kang,^{1,2} Soham Shah,³ Mingjie Xu,⁴ Toshihiro Aoki,⁴ Timothy J. Rupert,¹ Jian Luo,⁵ Kandis Leslie Gilliard-AbdulAziz,^{3,6} and William J. Bowman^{1,4,a)}

AFFILIATIONS

¹Department of Materials Science and Engineering, University of California Irvine, Irvine, California 92697, USA

²Department of Materials Science and Engineering, Yonsei University, Seoul 03722, South Korea

³Department of Chemical and Environmental Engineering, University of California Riverside, Riverside, California 92521, USA

⁴Irvine Materials Research Institute (IMRI), University of California Irvine, Irvine, California 92697, USA

⁵Department of NanoEngineering, University of California San Diego, La Jolla, California 92093, USA

⁶Department of Civil and Environmental Engineering, University of Southern California, Los Angeles, California 90089, USA

Note: This paper is part of the APL Special Collection on Era of Entropy: Synthesis, Structure, Properties, and Applications of High Entropy Materials.

^{a)} Author to whom correspondence should be addressed: will.bowman@uci.edu

ABSTRACT

Compositionally complex oxides (CCOs) are an emerging class of materials encompassing high entropy and entropy stabilized oxides. These promising advanced materials leverage tunable chemical bond structure, lattice distortion, and chemical disorder for unprecedented properties. Grain boundary (GB) and point defect segregation to GBs are relatively understudied in CCOs even though they can govern macroscopic material properties. For example, GB segregation can govern local chemical (dis)order and point defect distribution, playing a critical role in electrochemical reaction kinetics, and charge and mass transport in solid electrolytes. However, compared with conventional oxides, GBs in multi-cation CCO systems are expected to exhibit more complex segregation phenomena and, thus, prove more difficult to tune through GB design strategies. Here, GB segregation was studied in a model perovskite CCO $\text{LaFe}_{0.7}\text{Ni}_{0.1}\text{Co}_{0.1}\text{Cu}_{0.05}\text{Pd}_{0.05}\text{O}_{3-x}$ textured thin film by (sub-)atomic-resolution scanning transmission electron microscopy imaging and spectroscopy. It is found that GB segregation is correlated with cation reducibility—predicted by an Ellingham diagram—as Pd and Cu segregate to GBs rich in oxygen vacancies (V_{O}^{\bullet}). Furthermore, Pd and Cu segregation is highly sensitive to the concentration and spatial distribution of V_{O}^{\bullet} along the GB plane, as well as fluctuations in atomic structure and elastic strain induced by GB local disorder, such as dislocations. This work offers a perspective of controlling segregation concentration of CCO cations to GBs by tuning reducibility of CCO cations and oxygen deficiency, which is expected to guide GB design in CCOs.

Published under an exclusive license by AIP Publishing. <https://doi.org/10.1063/5.0202249>

Compositionally complex oxides (CCOs) are an emerging class of materials where multiple metals reside on the cation sublattice.^{1–3} CCOs include high entropy oxides (HEOs) and entropy stabilized oxides (ESOs), depending on how much the role of configurational entropy influences phase stability.^{2,4} High entropy oxides can form unique combinations of long-range crystallinity and local compositional disorder in the lattice.^{2,5} In oxides with oxygen-metal bonds,

factors such as the metal cation coordination number, bond length, angle, energy, degree of covalency, and vibration frequency are influenced by compositional complexity imposed through the distribution of metal cations, allowing tunability of functional properties, such as thermoelectric, dielectric, magnetic, electronic, ionic, thermal conductivity, and catalytic activity that are useful in energy storage and conversion.^{6–15}

Among various crystal structures, perovskites are fascinating candidates for high entropy design due to the existence of multiple cation sublattices, allowing a higher level of local compositional complexity.^{16–18} For example, perovskite structures can have both ordered and disordered cation sublattices, while anion sublattices remain ordered.^{19–22} The number of acceptor- or donor-type A or B cations in ABO_3 directly impacts charge carrier type and concentration, thereby charge transport.²³ Furthermore, the instability of perovskites under adverse conditions such as high temperature or high humidity can be enhanced by the addition of a range of cations with different activity levels in the lattice.^{9,24,25}

For electroceramics, in addition to chemical composition and crystal structure, defects, especially grain boundaries (GB), play an important role in their properties, e.g., they commonly serve as the rate-determined step for electrochemical processes.^{26–30} Ionic conduction in all-solid-state lithium-ion battery electrolytes and solid oxide fuel/electrolysis cells are severely restricted by the sluggish charge transport across GBs—caused by the relatively high conductivity activation energy barrier, low charge mobility, or low charge carrier concentration in space charge layers at/near GBs.^{31–35} Point defect segregation governs GB composition, chemical width, chemical order/disorder, electrostatic potential, and charge carrier distribution, which govern GB electrochemical properties.^{31,36–39}

Across material classes, segregation of solutes to GBs tends to reduce the total Gibbs free energy of the system, in which case this segregation is an equilibrium phenomenon.^{40–45} Equilibrium segregation is based on the intrinsic chemical properties of the system, while non-equilibrium segregation stems from systems' processing and thermal history; for example, elastic or electrostatic attraction between solutes and oxygen vacancies (V_O^\bullet) at the GB. Equilibrium segregation is typically driven by factors including the electrostatic potential at the grain boundary space charge layer. Elastic strain energy due to the lattice disorder (variation in size of solute and host atoms/ions) is another driving force, which creates lower energy GB sites for segregating solutes. One major segregation driving force is the difference in surface/bond energies, making CuO likely to segregate due to low surface/bond energies. Additionally, as demonstrated by this work, the cation reducibility is a governing factor.

Compared with conventional oxides containing a single solute/dopant cation, multi-cation CCO systems are expected to have a more complex GB structure.^{39,45–47} It is still not clear how GB segregation in CCOs is affected by local composition and atomic structures, such as V_O^\bullet concentration and local strain. Elucidating cation segregation phenomena in CCOs is important for further improving properties of CCOs through GB engineering, whereby macroscopic properties can be tuned by controlling GB composition resulting from synthesis and processing.

Transition metal elements commonly serve as constituents of CCOs, such as in electrochemical applications like electrocatalysis of the oxygen evolution reaction and electrodes of lithium-ion batteries. This is due to their partially occupied d-orbitals and tunable local coordination environment.^{48–50} Oxide GBs can be either oxygen deficient or oxygen rich,⁵¹ but they are usually viewed as a reservoir of V_O^\bullet , where their defect formation energy is much lower than in the adjacent grains.^{52,53} Control of V_O^\bullet concentration is also common during oxide synthesis, as we demonstrated recently by leveraging defect-interaction-driven exsolution of cations with high reducibility (in accordance

with the Ellingham model) during exsolution-self-assembly of Pd nanorods and Pd-Ni_xCo_{1-x}O core-shell nanoparticles during pulsed laser deposition (PLD) of CCO thin films.⁵⁴ Exsolution is a phase precipitation reaction that relies on cation reducibility and segregation, which in turn depends on the local V_O^\bullet concentration enrichment that drives cation coalescence and phase precipitation.^{52,55} It is also possible to leverage cation reducibility of ESOs to tune electronic conductivity, as we showed recently by modulating electronic conductivity by 10 000 times by reversibly precipitating Cu- and Cu-rich secondary phases from the rock salt ESO (Cu, Ni, Co, Mg, Zn)O.⁴⁷

Here, we thus hypothesize that the local reducing environment of GBs created by the accumulated V_O^\bullet associated with electrons released from oxygen Schottky defects facilitates cation GB segregation in CCOs. It is hypothesized that the cation segregation sequence is highly sensitive to relative cation reducibility, as predicted by the Ellingham diagram, meaning that cations with higher reducibility possess greater co-segregation tendency with V_O^\bullet driven by electrostatic point defect interactions. Additionally, the local spatial distribution of segregated cations is hypothesized to be governed by the local concentration and spatial distribution of V_O^\bullet at GBs, which are related to non-uniform GB atomic structures and local disorders that govern the V_O^\bullet formation energy along the GB plane. To test our hypotheses, a GB segregation study was done on a model textured perovskite CCO thin film of LaFe_{0.7}Ni_{0.1}Co_{0.1}Cu_{0.05}Pd_{0.05}O_{3-x} with five transition-metal constituents at the B site (Fig. S1) to decipher the role of cation reducibility, and concentration and V_O^\bullet distribution on GB segregation.

In this work, we fabricate a textured LaFe_{0.7}Ni_{0.1}Co_{0.1}Cu_{0.05}Pd_{0.05}O_{3-x} (CCO) thin film with (121)_{orthorhombic}|(110)_{pseudocubic} (pc) preferred orientation by depositing the perovskite CCO on a fluorite YSZ buffer layer using PLD^{48,56–61} [Figs. 1(a)–1(c)].⁶² GBs of the textured thin film can be observed under STEM^{26,63,64} by fabricating a plan-view specimen [Fig. 1(b)]. GBs form between columnar nanograins, and most of them are nearly parallel to the optic axis (i.e., edge-on orientation) in the STEM high-angle annular dark-field (HAADF) images^{27,40} [Fig. 1(d) and Figs. S2(a) and S2(b)], indicating most GB planes are parallel to the electron beam. The similar (110)_{pc} orientation of columnar nanograins facilitates observation of atomic arrangement at each side of the GBs [Fig. 1(e) and Fig. S2(c)].

It is found that Pd and Cu segregate at most GBs of the CCO from low-magnification STEM EDS mapping [Figs. 2(a)–2(f) and Figs. S3(a) and S3(b)]. To quantify GB chemistry, high-magnification STEM energy dispersive spectroscopy (EDS) mapping was done on a randomly selected GB [Figs. 2(g)–2(l) and Figs. S3(c) and S3(d)]. For the B-site cations at the GB, Pd and Cu show strong energy-dispersive x-ray spectroscopy (EDS) signal [Figs. 2(k) and 2(l)], Ni shows only a subtle change from the bulk behavior [Fig. S3(c)], Co is weakly deficient [Fig. S3(d)], while Fe is strongly deficient [Fig. 2(i)]. A-site cation La and anion O are also deficient at the GB [Figs. 2(h) and 2(j)]. The segregation width of Cu and Pd is around 1 nm from the composite EDS mapping [Fig. 2(m)], wider than the GB core structural width of 0.35 nm visible by HAADF [Fig. 2(g)].

Semi-quantitative EDS analysis was used to assess segregation and deficiency of each element at the CCO GB compared with the bulk grain—with assumed stoichiometry of LaFe_{0.7}Ni_{0.1}Co_{0.1}Cu_{0.05}Pd_{0.05}O_{3-x}. A simplified Cliff Lorimer K-factor method^{40,65,66} was used for concentration calculation, Eq. (1), where the concentration ratio of two elements ($\frac{C_A}{C_B}$) is proportional to their corresponding EDS

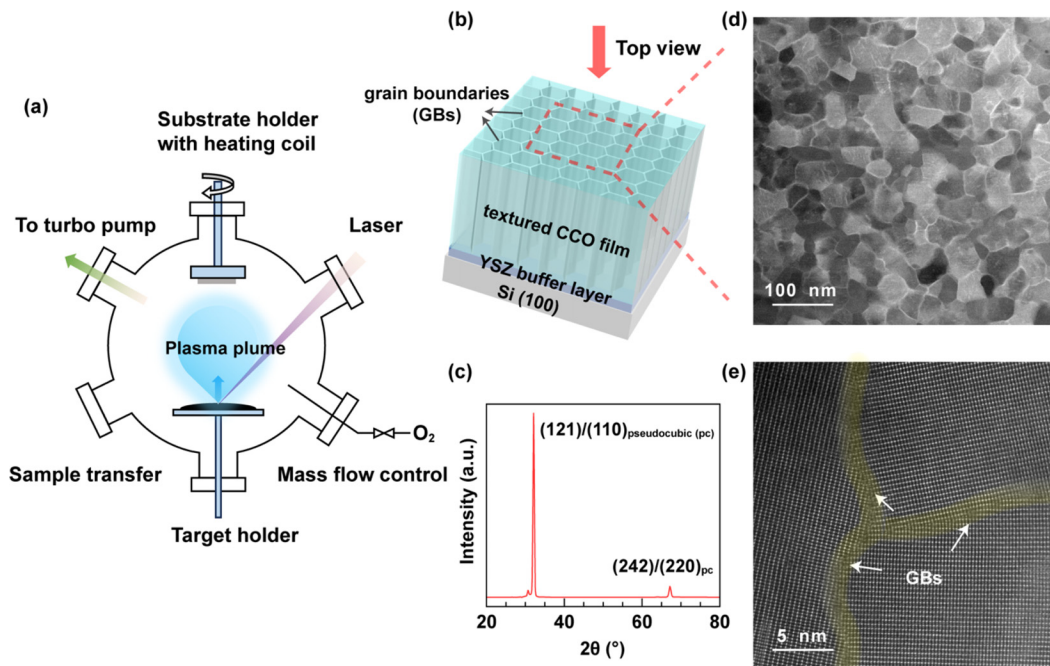


FIG. 1. Preparation of a plan-view textured perovskite CCO thin film for GB segregation study. (a) Pulsed laser deposition (PLD). (b) Textured CCO grown on Si (100) with YSZ buffer layer, with GBs between columnar grains. Plan-view TEM specimen (marked as a red rectangle). (c) XRD of the CCO thin film showing $(110)_{\text{pseudocubic(pc)}}$ texture; the left satellite peak of $(121)/(110)$ is from the tungsten source. (d) STEM HAADF showing GBs are sharp and clear. (e) STEM HAADF showing a triple junction between textured $(110)_{\text{pc}}$ grains.

signal intensity ratio ($\frac{I_A}{I_B}$) scaled by a factor k_{AB} . The EDS signal intensity profile of each element (Fig. S4) was extracted along the direction orthogonal to the GB plane, marked as an arrow in Fig. 2(h), and integrated over the entire EDS map area. Since EDS signals of Ni show subtle change across the GB [Figs. S3(c) and S4], it is assumed that Ni occupies 10% of the B-site at the GBs and in the grains (i.e., $C_{\text{Ni}} = 0.1$). Concentration profiles of each other element across the GB can be acquired by calculating its K-factor with Ni ($k_{X-\text{Ni}}$) at both side of grains (Table S1), and then obtaining its concentration ratio profile with Ni ($\frac{C_X}{C_{\text{Ni}}}$) using Eq. (1). The detailed calculation process is shown in Note S3 of the supplementary material,

$$\frac{C_A}{C_B} = k_{AB} \cdot \frac{I_A}{I_B}. \quad (1)$$

It is shown that the chemical composition of the GB is significantly different from the grain region, which approaches the stoichiometric ratio [Fig. 2(n)]. At the GB core marked as an arrow in Fig. 2(n), Pd and Cu show around 110% and 50% higher concentration than the stoichiometric ratio, respectively, while Co, La, Fe, and O show around 20%, 15%, 30%, and 20% lower concentration than the stoichiometric ratio, respectively. At the GB deficient with O, the concentration of segregated Pd is higher than that of Cu; Ni just shows subtle concentration change, while Co shows deficiency, which is less than Fe. This indicates that the amount of segregation at CCO GBs is correlated with the reducibility of cations as predicted by the Ellingham diagram, where Pd as the noble metal shows strongest reducibility, and Cu shows stronger reducibility than Ni, Co, and Fe as transition metals. Therefore, oxygen deficiency at GBs [Figs. 2(j) and 2(n)] may

attract cations with high reducibility, like Pd and Cu, to segregate preferentially since GBs may serve as a reservoir of V_{O}^{\bullet} because vacancy formation energies are lower than in the grains, thus forming a local reducing environment.^{53,67} This observation of preferential Pd segregation relative to less reducible transition metal cations was also observed in our prior work on this CCO during exsolution-self-assembly.⁵⁴

In addition to the segregation of Pd and Cu at GBs, it is also found that there is nonuniform distribution of Pd and Cu along the GB plane, where Pd and Cu aggregate at specific regions of GBs [Figs. 2(o)–2(u) and Figs. S3(e) and S3(f)]. This localized non-uniform segregation along the GB plane may arise from local disorder of GBs, such as dislocation cores and V_{O}^{\bullet} accumulation. Therefore, in addition to the chemical reducibility that governs the tendency of cation segregations, the local GB atomic structure defines the spatial distribution of cation segregation.

To prove that oxygen deficiency at GBs corresponds to the accumulation of V_{O}^{\bullet} , STEM EELS was used to track changes of the electronic structure of O at the GB and grains [Figs. 3(a) and 3(b) and Fig. S6]. The O-K edge pre-peak shows a significant decrease in intensity at the GB compared with the adjacent grains [highlighted yellow in Fig. 3(b) and Fig. S6]. The decrease in the O-K pre-edge intensity is regarded as appearance of V_{O}^{\bullet} since electrons released during formation of V_{O}^{\bullet} [Eq. (2)] partially fill the oxygen conduction band (or unoccupied orbitals), which will cause less electrons from core shells filling the conduction band, corresponding to weaker intensity of EELS signal at the O-K pre-edge.^{31,68–70} This EEL spectra change of O-K edge at GB correspond well with oxygen deficiency shown in the STEM EELS

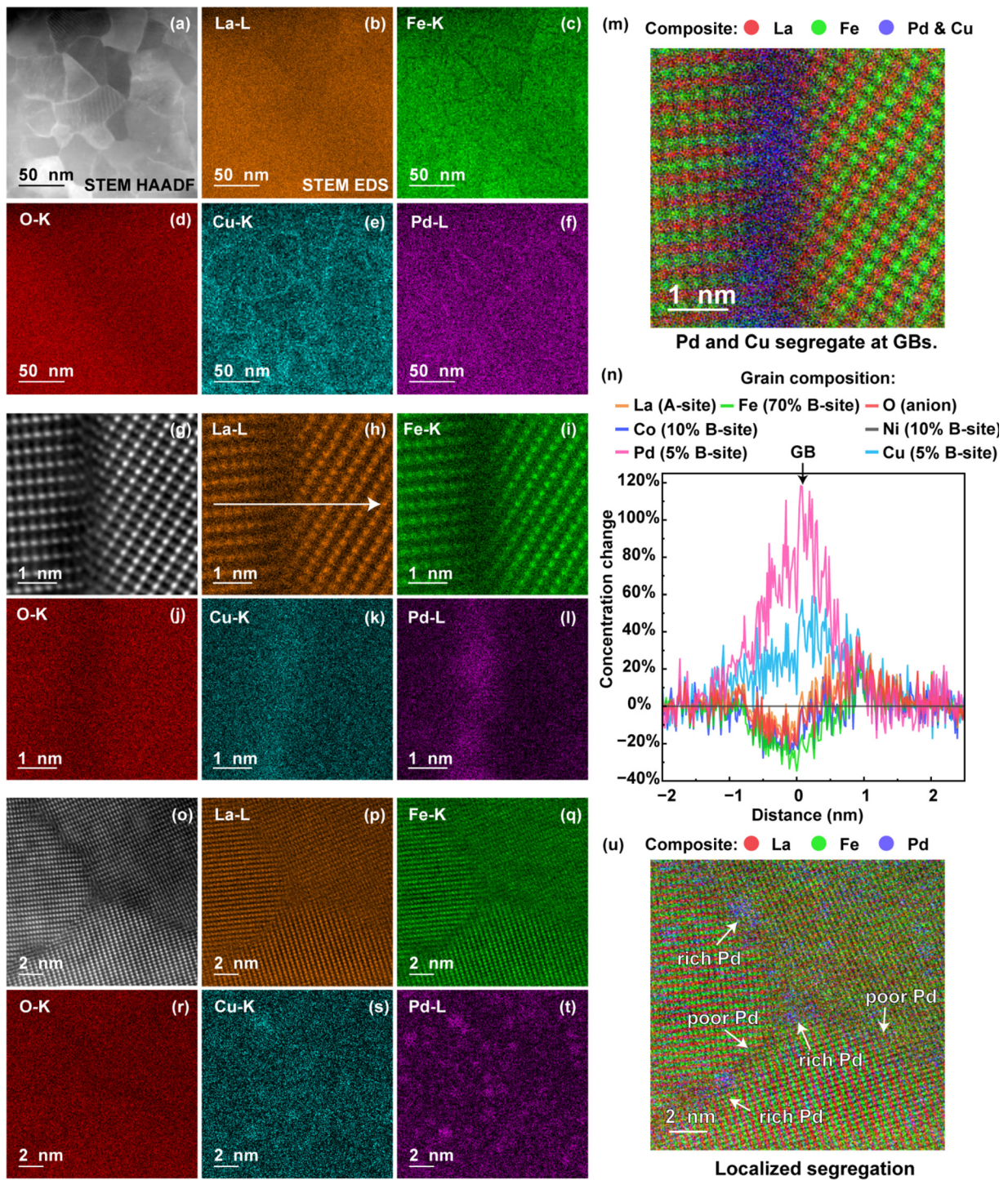


FIG. 2. Pd and Cu GB segregation. (a) STEM HAADF survey image; (b) La-L; (c) Fe-K; (d) O-K; (e) Cu-K; and (f) Pd-L. (g) STEM HAADF survey image; (h) La-L with filter; (i) Fe-K with filter; (j) O-K; (k) Cu-K; (l) Pd-K; and (m) composite of La (red), Fe (green), and mixed Cu and Pd (blue). (n) Concentration profiles across the GB in (g) perpendicular to the GB [white arrow in (h)]; integrated EDS signals were converted to concentration by K-factor method. (o) STEM HAADF survey image; (p) La-L with filter; (q) Fe-K with filter; (r) O-K; (s) Cu-K; (t) Pd-K; and (u) composite of La (red), Fe (green), and Pd (blue). The nonuniform distribution of Cu and Pd at GBs indicates that the localized GB structure may dominate dopant segregation.

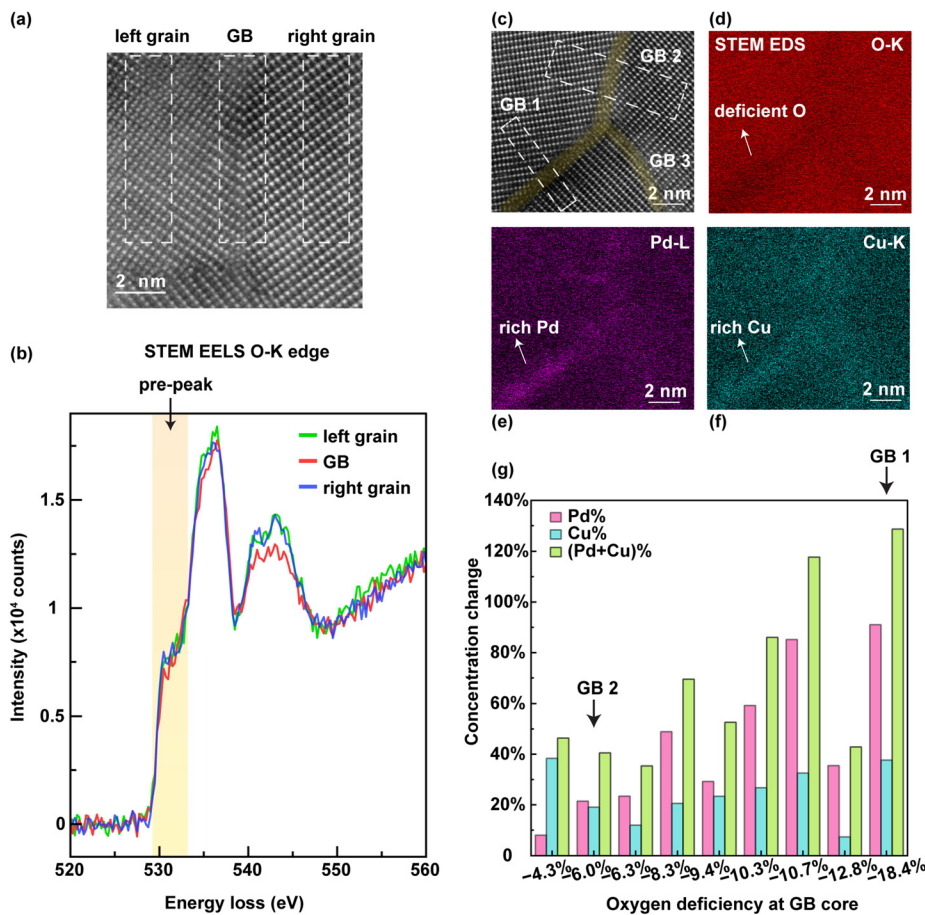
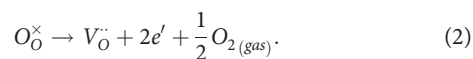


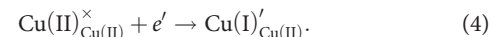
FIG. 3. Oxygen deficiency at GBs induces segregation of Pd and Cu. (a) STEM HAADF and (b) corresponding EEL spectra of the GB, left, and right grains in the rectangle regions. The EELS dispersion was 0.25 eV/channel. (c) STEM HAADF of a triple junction, and corresponding EDS of O (d), Pd (e), and Cu (f), showing oxygen deficiency correlates with Pd and Cu segregation. (g) Statistics on oxygen deficiency and Pd (pink), Cu (blue), and combined Cu and Pd (green) concentration at GBs from semi-quantitative EDS analysis on multiple GBs.

and EDS elemental mapping (Fig. S5), so the accumulated $V_{\text{O}}^{\bullet\bullet}$ at GBs induce segregation of cations with high reducibility in CCOs, such as Pd and Cu, due to their lower co-segregation energy with $V_{\text{O}}^{\bullet\bullet}$.^{71–73} The segregated Pd and Cu cations acquire electrons released from the formation of $V_{\text{O}}^{\bullet\bullet}$ to undergo reduction,



Therefore, the overall electrochemical model of the CCO GBs comprises defect reaction involving the formation of oxygen Schottky defects [Eq. (2)] and the electrochemical reducing reaction of cations, and both reactions take place simultaneously. Since we did not observe metal phase and other oxide phases, like PdO and Cu₂O, at the CCO GBs from the fast Fourier transfer (FFT) analysis from the GBs with significant segregation of Pd and Cu (Fig. S7), we believe the CCO GBs stay in the single phase, and segregated Cu and Pd at GBs are still involved in the perovskite phase, but their valence states get reduced to compensate the electrons released from $V_{\text{O}}^{\bullet\bullet}$ formation [Eqs. (3) and (4)]. In this electrochemical model, the co-segregation energy of cations with $V_{\text{O}}^{\bullet\bullet}$ will determine the order of cation segregation, which can be predicted with Ellingham diagram, while distribution and concentration of $V_{\text{O}}^{\bullet\bullet}$ determines the segregation concentration of each cation.

We attempted to use STEM EELS to track the valence change of Pd and Cu cations at the GB shown in Fig. 3(a). The local valence change of Cu cations across the CCO GB was observed by EELS, but the significant EEL spectrum overlap between La–M, Ni–L, and Cu–L, and the overlap between C–K and Pd–M, and lower doping concentration of Cu and Pd (5% of B-site cation individually) make it difficult to identify Cu–L and Pd–M and measure their valence states (Figs. S8–S12),



Additionally, it is found that different GBs show different segregation behavior. In the triple junction shown in Fig. 3(c), GB 1 shows much higher EDS signal of Pd and Cu and less EDS signal of O than GB 2 and GB 3 [Figs. 3(d)–3(f)]. This indicates that more severe oxygen deficiency may cause more Pd and Cu to segregate at GBs. The oxygen deficiency may show great deviations in GBs since even subtle change of 5 degrees of freedom, which describe misorientation and GB plane direction, and additional three microscopic degrees of freedom, which describe local atom arrangement, will create very different GB structures and vacancy formation energies.^{37,74,75} Therefore, semi-quantitative

EDS analysis was done on a series of nine GBs to decipher the variations of oxygen deficiency and its role in segregation concentration of Pd and Cu [Fig. 3(g)]. In the nine survey GBs, oxygen deficiency at the GB core varies from 4.3% to 18.4% relative to the stoichiometric concentration. The concentration of Pd, Cu, and combined Pd and Cu at the GB core tend upward with oxygen deficiency or V_{O}^{\bullet} accumulation, although exceptions exist in some GBs arising from specific GB structure [Fig. 3(g)]. Therefore, CCO GBs with higher concentration of V_{O}^{\bullet} will induce a greater number of reducible cations to segregate, which provides a perspective to engineer GBs to improve properties of CCOs because cation segregation concentration of CCOs can be controlled by modifying oxygen deficiency of GBs through CCO/HEO/ESO composition design, synthesis, and post-processing.

To track the role of localized strain in GB segregation, a low-angle tilt GB made up of a dislocation array was characterized with STEM EDS mapping, together with geometric phase analysis (GPA), which identifies lattice distortion around dislocation cores^{76–80}

[Figs. 4(a)–4(h)]. It is found that Pd and Cu locally segregate around the dislocation cores where the oxygen is deficient [Figs. 4(a)–4(f)]. The GPA shows that the extra-half atomic plane introduces intense compressive strain in surroundings and corresponding tensile strain at the other side of the dislocation core [Figs. 4(g) and 4(h)]. The profile of GB chemical change and strain distribution along the dislocation array, marked as an arrow in Fig. 4(b), indicates that the oxygen deficiency and corresponding Pd and Cu segregation are localized at the regions with strong strain, highlighted as yellow in Fig. 4(i). It has been reported that either compressive or tensile strain may decrease the formation energy of V_{O}^{\bullet} to enhance V_{O}^{\bullet} concentration at strained regions.^{68,81,82} Therefore, in this CCO system, cations with high reducibility prefer to segregate at strongly strained regions with locally accumulated V_{O}^{\bullet} .

To summarize, a textured thin film of a model perovskite CCO ($\text{LaFe}_{0.7}\text{Ni}_{0.1}\text{Co}_{0.1}\text{Cu}_{0.05}\text{Pd}_{0.05}\text{O}_{3-x}$) was prepared by PLD, and its plan-view specimen was used to decipher the role of CCO composition and GB atomic structure in cation segregation at GBs of this multi-cation

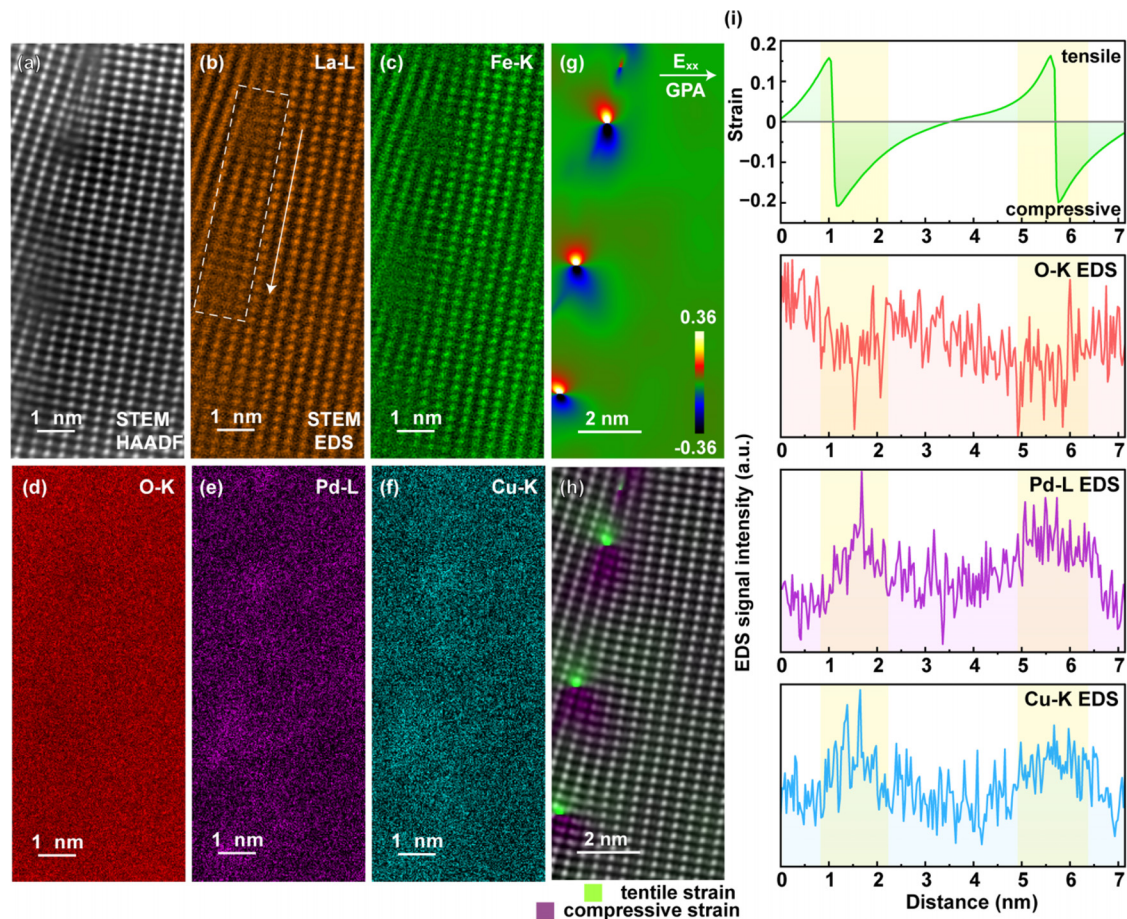


FIG. 4. Strain at dislocation cores induces localized oxygen deficiency and segregation of Cu and Pd. (a) STEM HAADF of a low-angle tilt GB made up of a dislocation array, and EDS of filtered La-L (b), filtered Fe-K (c), O-K (d), Pd-L (e), and Cu-K (f). (g) Strain mapping around this GB along the E_{xx} direction by geometric phase analysis (GPA), and composite of the inverse fast Fourier transform (IFFT) image and GPA strain mapping along E_{xx} direction showing atomic arrangement causing tensile (green) and compressive strain (purple). (i) Profile of strain and EDS signal along the dislocation array [arrow in (b)], with EDS signal in white rectangle. Strain correlated with oxygen deficiency and increased Pd and Cu intensity, highlighted as yellow.

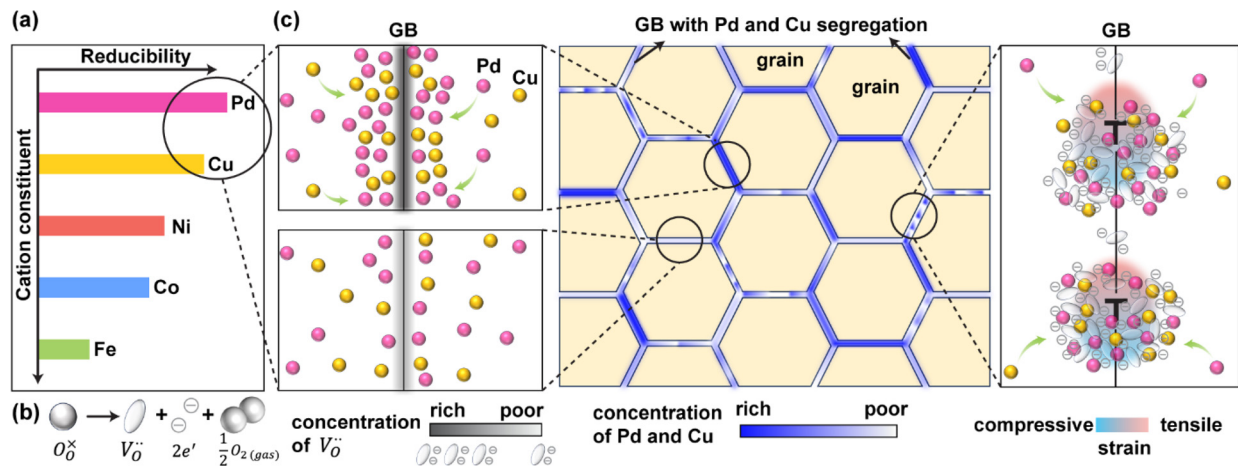


FIG. 5. The role of cation reducibility, oxygen deficiency, and localized strain in GB segregation. (a) More reducible Pd and Cu prefer to segregate at GBs with oxygen deficiency caused by (b) Schottky defects, where $V_O^{\bullet\bullet}$ and electrons occupy oxygen sites vacated by oxygen, forming gas at the surface. (c) Nonuniform Pd and Cu segregation may arise from varied oxygen deficiency along GBs. Pd and Cu segregation is affected by localized strain of $V_O^{\bullet\bullet}$ formation by lowering their formation energy.

system (Fig. 5). GB structure, chemistry and local disorder are probed by (sub)-nanoscale-resolution STEM associated with EDS, EELS, and GPA. Compared with Ni, Co, and Fe, the greater reducibility of Pd and Cu yield significant GB segregation closely correlated with oxygen deficiency, indicating cation reducibility governs the segregation concentration of the CCO GBs, which can be predicted by the Ellingham diagram [Fig. 5(a)]. Additionally, oxygen deficiency in the lattice arises from the formation of Schottky defects [Fig. 5(b)], so the oxygen deficiency at GBs corresponds to accumulation of $V_O^{\bullet\bullet}$, which was confirmed by tracking changes of the O-K edge EELS pre-peak. Therefore, accumulated $V_O^{\bullet\bullet}$ and electrons they released make GBs an environment compatible with cations with greater reducibility, leading them to segregate due to their low co-segregation energy of $V_O^{\bullet\bullet}$ [Figs. 5(b) and 5(c)]. In addition to compositions of CCOs, GB nanostructures also contribute to the cation segregation concentration by modifying the extent and distribution of oxygen deficiency [Fig. 5(c)]. Generally, concentration of Pd and Cu tend upward with oxygen deficiency or $V_O^{\bullet\bullet}$ accumulation. Strongly strained regions around dislocation cores facilitate the formation of $V_O^{\bullet\bullet}$ and thus induce localized segregation of Pd and Cu. This work introduces a perspective that cation segregation concentration of CCO GBs can be controlled by CCO composition through the incorporation of cations based on their Ellingham reducibility, and the extent and distribution of oxygen deficiency along the GB plane, which should broadly inform as the strategies to engineer GBs within the CCO community. In the future work, annealing pressure, temperature, and time will be considered to explore CCO GB segregation at a well-defined equilibrium state. Additionally, GB segregation in additional CCO systems with different crystal structures and constituents will be studied to further develop the CCO GB segregation model and improve tunability of segregation.

See the supplementary material for unit cell models of the perovskite CCO, STEM HAADF images of the plan-view CCO specimen, methods, notes on fabrication of PLD targets, XRD characterization on the CCO textured film, semi-quantitative EDS and EELS analysis, and FFT pattern analyses.

H.G. and W.J.B. acknowledge NSF CAREER (No. DMR-2042638) and ACS PRF (No. 61961-DNI). H.V., T.J.R., J.L., and W. J.B. were primarily supported by the National Science Foundation Materials Research Science and Engineering Center program through the UC Irvine Center for Complex and Active Materials (No. DMR-2011967). S.S. and K.L.G.-A. were primarily supported through the Center for Complex and Active Materials seed program. The authors acknowledge the use of facilities and instrumentation at the UC Irvine Materials Research Institute (IMRI), which is supported in part by the National Science Foundation through the UC Irvine Materials Research Science and Engineering Center (No. DMR-2011967).

AUTHOR DECLARATIONS

Conflict of Interest

The authors have no conflicts to disclose.

Author Contributions

Huiming Guo: Conceptualization (equal); Data curation (lead); Formal analysis (lead); Funding acquisition (lead); Investigation (lead); Methodology (equal); Project administration (lead); Resources (equal); Software (lead); Supervision (lead); Validation (equal); Visualization (lead); Writing – original draft (lead); Writing – review & editing (equal). **Hasti Vahidi:** Conceptualization (equal); Data curation (lead); Formal analysis (lead); Investigation (lead); Methodology (equal); Software (lead); Visualization (lead); Writing – original draft (equal); Writing – review & editing (equal). **Hyojoo Kang:** Conceptualization (equal); Formal analysis (equal); Writing – original draft (equal); Writing – review & editing (equal). **Soham Shah:** Formal analysis (equal); Investigation (equal); Methodology (equal); Writing – original draft (equal). **Mingjie Xu:** Investigation (equal); Methodology (equal); Resources (equal); Validation (equal); Writing – review & editing (equal). **Toshihiro Aoki:** Methodology (equal); Resources (equal); Software (equal); Validation (equal); Writing – review & editing (equal). **Timothy J. Rupert:** Conceptualization (equal); Resources

(equal); Software (equal); Validation (equal); Writing – review & editing (equal). **Jian Luo:** Conceptualization (equal); Validation (equal); Writing – review & editing (equal). **Kandis Leslie Gilliard-AbdulAziz:** Conceptualization (equal); Methodology (equal); Supervision (equal); Validation (equal); Writing – review & editing (equal). **William J. Bowman:** Conceptualization (equal); Funding acquisition (lead); Methodology (equal); Project administration (lead); Resources (equal); Supervision (lead); Validation (equal); Writing – original draft (supporting); Writing – review & editing (equal).

DATA AVAILABILITY

The data that support the findings of this study are available from the corresponding author upon reasonable request.

REFERENCES

- ¹X. Wang, J. Cortez, A. D. Dupuy, J. M. Schoenung, and W. J. Bowman, *Mater. Res. Lett.* **11**(3), 196 (2023).
- ²M. Brahlek, M. Gazda, V. Keppens, A. R. Mazza, S. J. McCormack, A. Mielewczyk-Gryn, B. Musico, K. Page, C. M. Rost, S. B. Sinnott, C. Toher, T. Z. Ward, and A. Yamamoto, *APL Mater.* **10**(11), 110902 (2022).
- ³A. J. Wright and J. Luo, *J. Mater. Sci.* **55**(23), 9812 (2020).
- ⁴A. J. Wright, Q. Wang, C. Huang, A. Nieto, R. Chen, and J. Luo, *J. Eur. Ceram. Soc.* **40**(5), 2120 (2020).
- ⁵S. S. Aamlid, M. Oudah, J. Rottler, and A. M. Hallas, *J. Am. Chem. Soc.* **145**(11), 5991 (2023).
- ⁶P. Zhang, Z. Lou, M. Qin, J. Xu, J. Zhu, Z. Shi, Q. Chen, M. J. Reece, H. Yan, and F. Gao, *J. Mater. Sci. Technol.* **97**, 182 (2022).
- ⁷W. Xiong, H. Zhang, S. Cao, F. Gao, P. Svec, J. Dusza, M. J. Reece, and H. Yan, *J. Eur. Ceram. Soc.* **41**(4), 2979 (2021).
- ⁸L. Su, H. Huyan, A. Sarkar, W. Gao, X. Yan, C. Addiego, R. Kruk, H. Hahn, and X. Pan, *Nat. Commun.* **13**(1), 2358 (2022).
- ⁹Y. Shi, N. Ni, Q. Ding, and X. Zhao, *J. Mater. Chem. A* **10**(5), 2256 (2022).
- ¹⁰D. Bérardan, S. Franger, A. K. Meena, and N. Dragoe, *J. Mater. Chem. A* **4**(24), 9536 (2016).
- ¹¹L. Xu, L. Su, H. Wang, H. Gao, D. Lu, K. Peng, M. Niu, and Z. Cai, *J. Am. Ceram. Soc.* **105**(2), 1548 (2022).
- ¹²C. Deng, T. Wang, P. Wu, W. Zhu, and S. Dai, *Nano Energy* **120**, 109153 (2024).
- ¹³A. Sarkar, L. Velasco, D. Wang, Q. Wang, G. Talasila, L. de Biasi, C. Kübel, T. Brezesinski, S. S. Bhattacharya, H. Hahn, and B. Breitung, *Nat. Commun.* **9**(1), 3400 (2018).
- ¹⁴R. Zhang, C. Wang, P. Zou, R. Lin, L. Ma, L. Yin, T. Li, W. Xu, H. Jia, Q. Li, S. Sainio, K. Kisslinger, S. E. Trask, S. N. Ehrlich, Y. Yang, A. M. Kiss, M. Ge, B. J. Polzin, S. J. Lee, W. Xu, Y. Ren, and H. L. Xin, *Nature* **610**(7930), 67 (2022).
- ¹⁵Y. Zeng, B. Ouyang, J. Liu, Y.-W. Byeon, Z. Cai, L. J. Miara, Y. Wang, and G. Ceder, *Science* **378**(6626), 1320 (2022).
- ¹⁶Y. Wang, J. Liu, Y. Song, J. Yu, Y. Tian, M. J. Robson, J. Wang, Z. Zhang, X. Lin, G. Zhou, Z. Wang, L. Shen, H. Zhao, S. Grasso, and F. Ciucci, *Small Methods* **7**(4), 2201138 (2023).
- ¹⁷S. Jiang, T. Hu, J. Gild, N. Zhou, J. Nie, M. Qin, T. Harrington, K. Vecchio, and J. Luo, *Scr. Mater.* **142**, 116 (2018).
- ¹⁸D. Chen, S. Nie, L. Wu, X. Zheng, S. Du, X. Duan, Q. Niu, P. Zhang, and S. Dai, *Chem. Mater.* **34**(4), 1746 (2022).
- ¹⁹J. Luong, X. Wang, A. Tsung, N. Humphrey, H. Guo, B. X. Lam, S. Mallikarjun Sharada, and W. J. Bowman, *ACS Appl. Nano Mater.* **6**(3), 1620 (2023).
- ²⁰T. Wang, H. Chen, Z. Yang, J. Liang, and S. Dai, *J. Am. Chem. Soc.* **142**(10), 4550 (2020).
- ²¹T. Erdil and C. Toparli, *ACS Appl. Energy Mater.* **6**(21), 11255 (2023).
- ²²A. Sarkar, R. Djenadic, D. Wang, C. Hein, R. Kautenburger, O. Clemens, and H. Hahn, *J. Eur. Ceram. Soc.* **38**(5), 2318 (2018).
- ²³Y. Wang, M. J. Robson, A. Manzotti, and F. Ciucci, *Joule* **7**(5), 848 (2023).
- ²⁴Z. Liu, Z. Tang, Y. Song, G. Yang, W. Qian, M. Yang, Y. Zhu, R. Ran, W. Wang, W. Zhou, and Z. Shao, *Nano-Micro Lett.* **14**(1), 217 (2022).
- ²⁵D. Zhang, H. A. De Santiago, B. Xu, C. Liu, J. A. Trindell, W. Li, J. Park, M. A. Rodriguez, E. N. Coker, J. D. Sugar, A. H. McDaniel, S. Lany, L. Ma, Y. Wang, G. Collins, H. Tian, W. Li, Y. Qi, X. Liu, and J. Luo, *Chem. Mater.* **35**(5), 1901 (2023).
- ²⁶H. Vahidi, K. Syed, H. Guo, X. Wang, J. L. Wardini, J. Martinez, and W. J. Bowman, *Crystals* **11**, 878 (2021).
- ²⁷W. J. Bowman, J. Zhu, R. Sharma, and P. A. Crozier, *Solid State Ionics* **272**, 9 (2015).
- ²⁸E. Milan and M. Pasta, *Mater. Futures* **2**(1), 013501 (2023).
- ²⁹X. Liu, R. Garcia-Mendez, A. R. Lupini, Y. Cheng, Z. D. Hood, F. Han, A. Sharafi, J. C. Idrobo, N. J. Dudney, C. Wang, C. Ma, J. Sakamoto, and M. Chi, *Nat. Mater.* **20**(11), 1485 (2021).
- ³⁰X. Xu, Y. Liu, J. Wang, D. Isheim, V. P. Dravid, C. Phatak, and S. M. Haile, *Nat. Mater.* **19**(8), 887 (2020).
- ³¹W. J. Bowman, M. N. Kelly, G. S. Rohrer, C. A. Hernandez, and P. A. Crozier, *Nanoscale* **9**(44), 17293 (2017).
- ³²A. Bokov, J. A. Aguiar, M. L. Gong, A. Nikonov, and R. H. R. Castro, *J. Phys. Chem. C* **122**(46), 26344 (2018).
- ³³X. Guo and R. Waser, *Prog. Mater. Sci.* **51**(2), 151 (2006).
- ³⁴T. Polczyk, W. Zając, M. Ziąbka, and K. Świerczek, *J. Mater. Sci.* **56**(3), 2435 (2021).
- ³⁵T. Lee, J. Qi, C. A. Gadre, H. Huyan, S.-T. Ko, Y. Zuo, C. Du, J. Li, T. Aoki, R. Wu, J. Luo, S. P. Ong, and X. Pan, *Nat. Commun.* **14**(1), 1940 (2023).
- ³⁶W. J. Bowman, A. Darbal, and P. A. Crozier, *ACS Appl. Mater. Interfaces* **12**(1), 507 (2020).
- ³⁷X. Tong, W. J. Bowman, A. Mejia-Giraldo, P. A. Crozier, and D. S. Mebane, *J. Phys. Chem. C* **124**(43), 23619 (2020).
- ³⁸M. Kindelmann, S. Escolastico, L. Almar, A. Vayyala, D. Jennings, W. Deibert, W. A. Meulenber, W. Rheinheimer, M. Bram, J. M. Serra, J. Mayer, and O. Guillon, ChemRxiv (2023).
- ³⁹S.-T. Ko, T. Lee, J. Qi, D. Zhang, W.-T. Peng, X. Wang, W.-C. Tsai, S. Sun, Z. Wang, W. J. Bowman, S. P. Ong, X. Pan, and J. Luo, *Matter* **6**(7), 2395 (2023).
- ⁴⁰K. Syed, M. Xu, K. K. Ohtaki, D. Kok, K. K. Karandikar, O. A. Graeve, W. J. Bowman, and M. L. Mecartney, *Materials* **14**, 100890 (2020).
- ⁴¹K. Syed, N. B. Motley, and W. J. Bowman, *Acta Mater.* **227**, 117685 (2022).
- ⁴²P. Wynblatt, G. S. Rohrer, and F. Papillon, *J. Eur. Ceram. Soc.* **23**(15), 2841 (2003).
- ⁴³N. D. Browning, R. F. Klie, and Y. Lei, presented at the Mixed Ionic Electronic Conducting Perovskites for Advanced Energy Systems, Dordrecht, 2004.
- ⁴⁴J. Nowotny, C. C. Sorrell, and T. Bak, *Surf. Interface Anal.* **37**(3), 316 (2005).
- ⁴⁵M. J. McCarthy, H. Zheng, D. Apelian, W. J. Bowman, H. Hahn, J. Luo, S. P. Ong, X. Pan, and T. J. Rupert, *Phys. Rev. Mater.* **5**(11), 113601 (2021).
- ⁴⁶J. Luo and N. Zhou, *Commun. Mater.* **4**(1), 7 (2023).
- ⁴⁷H. Vahidi, A. D. Dupuy, B. X. Lam, J. Cortez, P. Garg, T. J. Rupert, J. M. Schoenung, and W. J. Bowman, *Adv. Funct. Mater.* (published online 2024).
- ⁴⁸W. Li, J. Shi, K. H. L. Zhang, and J. L. MacManus-Driscoll, *Mater. Horiz.* **7**(11), 2832 (2020).
- ⁴⁹M. V. Kante, M. L. Weber, S. Ni, I. C. G. van den Bosch, E. van der Minne, L. Heymann, L. J. Falling, N. Gauquelin, M. Tsvetanova, D. M. Cunha, G. Koster, F. Gunkel, S. Nemsák, H. Hahn, L. Velasco Estrada, and C. Baeumer, *ACS Nano* **17**(6), 5329 (2023).
- ⁵⁰J. Baek, M. D. Hossain, P. Mukherjee, J. Lee, K. T. Winther, J. Leem, Y. Jiang, W. C. Chueh, M. Bajdich, and X. Zheng, *Nat. Commun.* **14**(1), 5936 (2023).
- ⁵¹Q. Yan, C. Hu, and J. Luo, *Mater. Today* **73**, 66 (2024).
- ⁵²K. Syed, J. Wang, B. Yildiz, and W. J. Bowman, *Nanoscale* **14**(3), 663 (2022).
- ⁵³D. Mutter, C. Tao, D. F. Urban, and C. Elsässer, *Adv. Eng. Mater.* **25**(18), 2201847 (2023).
- ⁵⁴H. Guo, C. Mead, M. Balingit, S. Shah, X. Wang, M. Xu, I. Tran, T. Aoki, J. D. Samaniego, K. L. Gilliard-AbdulAziz, L. J. Laughton, and W. J. Bowman, *Matter* **7**, 1002–1017 (2024).
- ⁵⁵J. Wang, K. Syed, S. Ning, I. Waluyo, A. Hunt, E. J. Crumlin, A. K. Opitz, C. A. Ross, W. J. Bowman, and B. Yildiz, *Adv. Funct. Mater.* **32**(9), 2108005 (2022).
- ⁵⁶N. A. Shepelin, Z. P. Tehrani, N. Ohannessian, C. W. Schneider, D. Pergolesi, and T. Lippert, *Chem. Soc. Rev.* **52**(7), 2294 (2023).
- ⁵⁷H. Guo, X. Wang, A. D. Dupuy, J. M. Schoenung, and W. J. Bowman, *J. Mater. Res.* **37**(1), 124 (2022).
- ⁵⁸R. Xie, X. Hu, Y. Shi, Z. Nie, N. Zhang, E. Traversa, Y. Yu, and N. Yang, *ACS Appl. Energy Mater.* **3**(8), 7988 (2020).

- ⁵⁹J. L. MacManus-Driscoll, M. P. Wells, C. Yun, J.-W. Lee, C.-B. Eom, and D. G. Schlom, *APL Mater.* **8**(4), 040904 (2020).
- ⁶⁰H. Han, J. Park, S. Y. Nam, K. J. Kim, G. M. Choi, S. S. P. Parkin, H. M. Jang, and J. T. S. Irvine, *Nat. Commun.* **10**(1), 1471 (2019).
- ⁶¹J. Wang, J. Yang, A. K. Opitz, W. Bowman, R. Bliem, G. Dimitrakopoulos, A. Nanning, I. Waluyo, A. Hunt, J.-J. Gallet, and B. Yildiz, *Chem. Mater.* **33**(13), 5021 (2021).
- ⁶²G. F. Harrington, L. Sun, B. Yildiz, K. Sasaki, N. H. Perry, and H. L. Tuller, *Acta Mater.* **166**, 447 (2019).
- ⁶³J. L. Wardini, H. Vahidi, H. Guo, and W. J. Bowman, *Front. Chem.* **9**, 743025 (2021).
- ⁶⁴J. Wang, A. Kumar, J. L. Wardini, Z. Zhang, H. Zhou, E. J. Crumlin, J. T. Sadowski, K. B. Woller, W. J. Bowman, J. M. LeBeau, and B. Yildiz, *Nano Lett.* **22**(13), 5401 (2022).
- ⁶⁵G. W. Lorimer, *Miner. Mag.* **51**(359), 49 (1987).
- ⁶⁶G. Cliff and G. W. Lorimer, *J. Microsc.* **103**(2), 203 (1975).
- ⁶⁷X. Tong, D. S. Mebane, and R. A. De Souza, *J. Am. Ceram. Soc.* **103**(1), 5 (2020).
- ⁶⁸S.-Y. Choi, S.-D. Kim, M. Choi, H.-S. Lee, J. Ryu, N. Shibata, T. Mizoguchi, E. Tochigi, T. Yamamoto, S.-J. L. Kang, and Y. Ikuhara, *Nano Lett.* **15**(6), 4129 (2015).
- ⁶⁹D. Pang, W. Li, N. Zhang, H. He, S. Mao, Y. Chen, L. Cao, C. Li, A. Li, and X. Han, *J. Rare Earths* **42**(4), 676 (2024).
- ⁷⁰N. Biskup, J. Salafranca, V. Mehta, M. P. Oxley, Y. Suzuki, S. J. Pennycook, S. T. Pantelides, and M. Varela, *Phys. Rev. Lett.* **112**(8), 087202 (2014).
- ⁷¹S. Joo, A. Seong, O. Kwon, K. Kim, J. H. Lee, R. J. Gorte, J. M. Vohs, J. Woo Han, and G. Kim, *Sci. Adv.* **6**(35), eabb1573 (2020).
- ⁷²O. Kwon, S. Sengodan, K. Kim, G. Kim, H. Y. Jeong, J. Shin, Y.-W. Ju, J. W. Han, and G. Kim, *Nat. Commun.* **8**(1), 15967 (2017).
- ⁷³S. Chae, L. Williams, J. Lee, J. T. Heron, and E. Kioupakis, *npj Comput. Mater.* **8**(1), 95 (2022).
- ⁷⁴D. Aksoy, H. L. Xin, T. J. Rupert, and W. J. Bowman, *arXiv:2312.09968* (2023).
- ⁷⁵J. Han, S. L. Thomas, and D. J. Srolovitz, *Prog. Mater. Sci.* **98**, 386 (2018).
- ⁷⁶S. Turner, H. Idrissi, A. F. Sartori, S. Korneychuck, Y. G. Lu, J. Verbeeck, M. Schreck, and G. Van Tendeloo, *Nanoscale* **8**(4), 2212 (2016).
- ⁷⁷P. Ren, M. Song, J. Lee, J. Zheng, Z. Lu, M. Engelhard, X. Yang, X. Li, D. Kisailus, and D. Li, *Adv. Mater. Interfaces* **6**(17), 1901121 (2019).
- ⁷⁸M. Takeda and J. Suzuki, *J. Opt. Soc. Am. A* **13**(7), 1495 (1996).
- ⁷⁹M. J. Hÿtch, E. Snoeck, and R. Kilaas, *Ultramicroscopy* **74**(3), 131 (1998).
- ⁸⁰H. Du, GPA: Geometric Phase Analysis software (2018).
- ⁸¹L. Sun, D. Marrocchelli, and B. Yildiz, *Nat. Commun.* **6**(1), 6294 (2015).
- ⁸²D. Marrocchelli, L. Sun, and B. Yildiz, *J. Am. Chem. Soc.* **137**(14), 4735 (2015).